

# Facile One-step Synthesis of $\text{Zn}_{1-x}\text{Mn}_x\text{SiN}_2$ Nitride Semiconductor Solid Solutions via Solid-state Metathesis Reaction

Otto E. O. Zeman,<sup>[a]</sup> Fabian O. von Rohr,<sup>[b]</sup> Lukas Neudert,<sup>[a]</sup> and Wolfgang Schnick\*<sup>[a]</sup>

**Abstract.** We report on the synthesis of the II-IV-N<sub>2</sub> semiconductors ZnSiN<sub>2</sub>, MnSiN<sub>2</sub>, and the  $\text{Zn}_{1-x}\text{Mn}_x\text{SiN}_2$  solid solutions by a one-step solid-state metathesis reaction. The successful syntheses were carried out by reacting the corresponding metal halides with stoichiometric amounts of silicon nitride and lithium azide in sealed tantalum ampoules. After washing out the reaction byproduct LiCl, powder X-ray diffraction patterns were indexed with orthorhombic space group *Pna2*<sub>1</sub>. Single phase products were obtained without applying external pressure and at a moderate reaction temperature of 700 °C. The re-

sulting ZnSiN<sub>2</sub> was found to consist of nano-sized grains and needle-shaped nano-crystals. With increasing manganese content in the  $\text{Zn}_{1-x}\text{Mn}_x\text{SiN}_2$  solid solution, we found the reaction product to be increasingly crystalline. Both the cell parameters and the bandgap values across the different compositions of the solid solutions change linearly. The sample  $\text{Zn}_{0.95}\text{Mn}_{0.05}\text{SiN}_2$  synthesized by means of solid-state metathesis reaction is an intense red emitter with a broad emission maximum at  $\lambda_{\text{max}} \approx 619$  nm when excited with ultraviolet light after annealing the sample at a pressure of 6 GPa and a temperature of 1200 °C.

## Introduction

Grimm-Sommerfeld type III-V semiconductors have become indispensable for many forefront semiconductor technologies. These materials are regularly used for optoelectronic applications, such as solid-state lasers,<sup>[1]</sup> light-emitting diodes,<sup>[2]</sup> and photovoltaics.<sup>[3]</sup> In particular, the material gallium nitride, GaN, and its respective solid solutions (Al,Ga,In)N are most essential for various applications. All of these compounds are structural and electronic analogues to the group IV element silicon, which is the pillar for almost all semiconductor electronics. Due to the scarcity of gallium, synthesis and investigation of the II-IV-V<sub>2</sub> materials, which are themselves structurally and electronically closely related to the III-V semiconductors, have recently become of great interest.<sup>[4]</sup>

The II-IV-V<sub>2</sub> compounds crystallize in space group *Pna2*<sub>1</sub>, the crystal structure and its group-subgroup relation to the wurtzite structure type with space group *P6*<sub>3</sub>*mc* are summarized in Figure 1a. The II-IV-V<sub>2</sub> compounds can be synthesized for a broad variety of different elemental compositions, all of which are semiconductors with bandgap values that span over a wide range between 0.4 and 5.7 eV. The lattice con-

stants of the II-IV-V<sub>2</sub> compounds are similar to those of the respective III-V semiconductors and to those of silicon, enabling the construction of hybrid devices.<sup>[5–8]</sup>

Of particular interest are the II-IV-V<sub>2</sub> nitridosilicates, nitridogermanates and nitridostannates (IV = Si, Ge, Sn) which feature similar structural, optical and electronic properties as the (Al,Ga,In)N compounds.<sup>[9]</sup> The compound MnSiN<sub>2</sub> takes a special role among the known II-IV-V<sub>2</sub> nitridosilicates. It is the only open-shell transition metal nitridosilicate, which crystallizes in a wurtzite-related structure. MnSiN<sub>2</sub> was found to display remarkably robust *anti*-ferromagnetic ordering with an exceptionally high Néel temperature for Mn<sup>2+</sup> compounds of  $T_N \approx 490$  K. It was furthermore found that a substantial amount of magnetic frustration must be present in this material.<sup>[10]</sup> The Zn-IV-N<sub>2</sub> nitrides span over a range of lattice constants and bandgaps, from 1.4 eV for ZnSnN<sub>2</sub> to 4 eV for ZnSiN<sub>2</sub>.<sup>[11–13]</sup> Among the II-IV-N<sub>2</sub> compounds, the zinc nitridosilicate ZnSiN<sub>2</sub> has so far only been scarcely investigated, due to the challenging accessibility of the material. ZnSiN<sub>2</sub> has a bandgap of approximately 4 eV, and its ratio of lattice constants to bandgap falls right between those of AlN and GaN. It, furthermore, displays an excellent electronic band-structure tunability, which can be modified by chemical substitution. Last but not least, it consists of earth-abundant elements and has been found to be rather stable in air and at elevated temperatures. However, the synthesis of ZnSiN<sub>2</sub> has been found to be challenging. The compound has so far only been obtained by three highly specialized, onerous syntheses methods: Initially, ZnSiN<sub>2</sub> was obtained by high-pressure/high-temperature synthesis technique using a belt-type apparatus at a pressure of 6.5 GPa and a temperature of 1500 °C starting from Zn<sub>3</sub>N<sub>2</sub> and Si<sub>3</sub>N<sub>4</sub>.<sup>[14]</sup> Zn<sub>3</sub>N<sub>2</sub> was prepared via an ammonia gas stream reaction, while the resulting nitride is not stable in air or at temperatures above 500 °C. Secondly, ZnSiN<sub>2</sub> has been synthesized as deposited thin films by metalorganic vapor phase epitaxy (MOVPE) or molecular beam epitaxy (MBE) tech-

\* Prof. Dr. Wolfgang Schnick  
E-Mail: wolfgang.schnick@uni-muenchen.de

[a] Department of Chemistry  
University of Munich (LMU)  
Butenandtstraße 5–13  
81377 Munich, Germany

[b] Department of Chemistry  
University of Zurich  
Winterthurerstraße 190  
8057 Zurich, Switzerland

Supporting information for this article is available on the WWW under <http://dx.doi.org/10.1002/zaac.201900315> or from the author.

© 2020 The Authors. Published by Wiley-VCH Verlag GmbH & Co. KGaA. • This is an open access article under the terms of the Creative Commons Attribution-NonCommercial-NoDerivs License, which permits use and distribution in any medium, provided the original work is properly cited, the use is non-commercial and no modifications or adaptations are made.

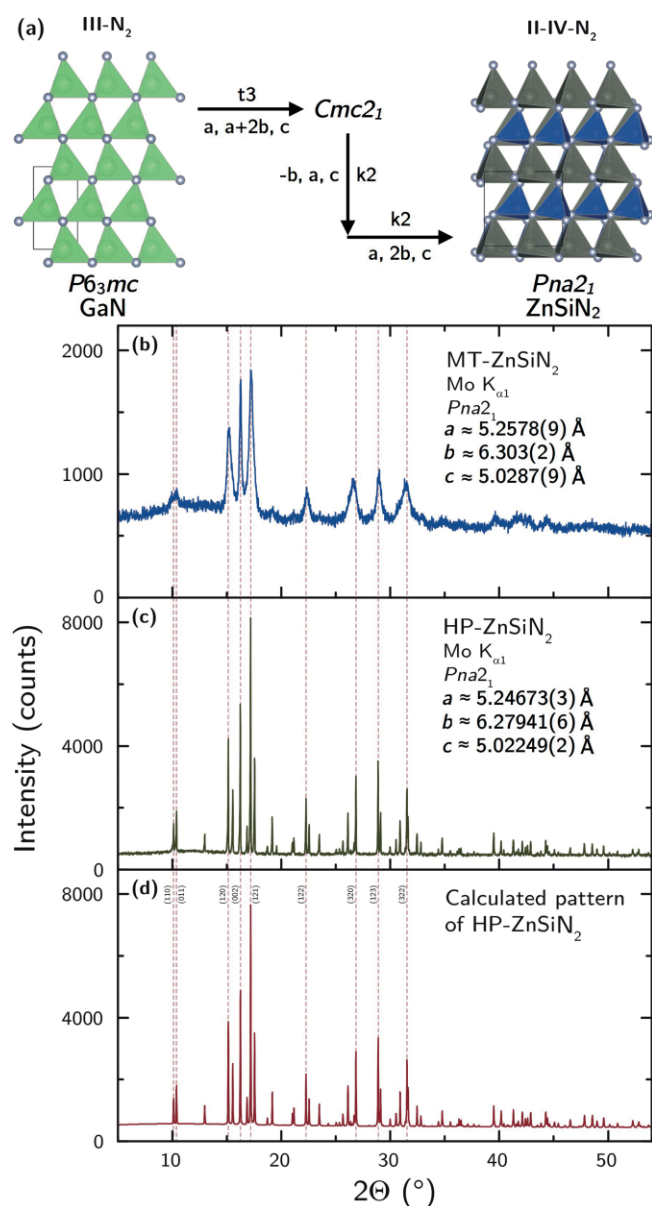


**Figure 1.** (a) Structure and subgroup relations of the compounds GaN and ZnSiN<sub>2</sub>.<sup>[21]</sup> (b) PXRD pattern of MT-ZnSiN<sub>2</sub> in blue and of (c) HP-ZnSiN<sub>2</sub> in green with some of the most prominent reflections marked with dotted red lines. (d) Calculated PXRD pattern of HP-ZnSiN<sub>2</sub> with the most prominent reflections indexed.

niques.<sup>[15]</sup> Thirdly, ZnSiN<sub>2</sub> is accessible by an ammonothermal approach using super-critical ammonia as the solvent at 600 °C in custom made autoclaves.<sup>[16,17]</sup>

Herein, we report on a facile, one-step synthesis method with which ZnSiN<sub>2</sub>, MnSiN<sub>2</sub>, and the entire solid solution series Zn<sub>1-x</sub>Mn<sub>x</sub>SiN<sub>2</sub> can be prepared without applying external pressure, using ZnCl<sub>2</sub> as zinc source. We furthermore show how the bandgap evolves within this system, and compare our results to high-pressure annealed, highly-crystalline HP-ZnSiN<sub>2</sub>.

## Experimental Section

Due to the starting materials' high sensitivity to moisture and oxygen, all reagents were handled in an argon-filled glovebox (Unilab, MBraun, Garching, O<sub>2</sub> < 1 ppm, H<sub>2</sub>O < 1 ppm). Representatives of the solid solution series with the general sum formula Zn<sub>1-x</sub>Mn<sub>x</sub>SiN<sub>2</sub> were synthesized in sealed tantalum ampoules. The starting materials MnCl<sub>2</sub> (Alfa Aesar, 99.99%), ZnCl<sub>2</sub> (Alfa Aesar, 99.99%), Si<sub>3</sub>N<sub>4</sub> (UBE, SN-E10) and LiN<sub>3</sub> (synthesized according to the method reported by Hofman-Bang)<sup>[18]</sup> were mixed with an agate mortar in stoichiometric amounts and filled into tantalum ampoules that subsequently were weld shut and heated in evacuated silica tubes to 900 °C in 5 h. The temperature was kept for 24 h and then cooled down to room temperature within 5 h. To remove LiCl, the resulting powders were washed with water and subsequently dried under air. All synthesized samples are insensitive towards the reaction with water and oxygen. Annealing of ZnSiN<sub>2</sub> was done at a pressure of 6 GPa and a temperature of 1200 °C for 1 h using a Walker-type multianvil assembly.<sup>[19]</sup>

Powder X-ray diffraction data were collected on a STOE Stadi P diffractometer with Mo-K<sub>α1</sub> radiation (λ = 0.7107 Å) in parafocusing Debye-Scherrer setup with a Ge(111) monochromator and a Mythen 1 K detector. Samples were ground and sealed in a glass capillary with 0.3 mm inner diameter and 0.01 mm wall thickness (Hilgenberg, Germany). LeBail-extractions were performed with the GSAS-II crystallographic software package.<sup>[20]</sup>

Transmission electron microscopy (TEM) investigations were performed on finely ground samples of ZnSiN<sub>2</sub>, which were dispersed in absolute ethanol and drop-casted on copper finder grids coated with a holey carbon film (S166-2, Plano GmbH, Germany). The grids were fixed on a double-tilt holder and investigated in a FEI Titan Themis 60–300 equipped with a monochromator, Cs-corrector and windowless, 4-quadrant EDX-detector. The TEM was operated at 300 kV and the images were recorded using 4k\*4k FEI Ceta CEMOS-CCD camera. SAED data were evaluated using the programs Digital Micrograph and JEMS. EDX data were processed with ES Vision.

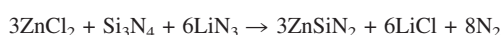
UV/Vis measurements on powder samples were conducted in PTFE sample holders on a Jasco V-650 UV/Vis spectrophotometer equipped with two 500 mm Czerny-Turner monochromators, 1800 1/mm lattices, and 250/500 nm lamps, with a spectral range from 230 to 800 nm.

**Supporting Information** (see footnote on the first page of this article): Diffuse reflectance spectra of Zn<sub>1-x</sub>Mn<sub>x</sub>SiN<sub>2</sub> for x = 0.0, 0.2, 0.4, 0.6, 0.8, 1.0.

## Results and Discussion

### PXRD Pattern of ZnSiN<sub>2</sub>

Figure 1b–d display the powder XRD patterns of the ZnSiN<sub>2</sub>, (b) synthesized by metathesis reaction pathway (in the following denoted as MT-ZnSiN<sub>2</sub>), (c) by a high-pressure and high-temperature annealing route (in the following denoted as HP-ZnSiN<sub>2</sub>), and (d) the calculated PXRD pattern of the HP-ZnSiN<sub>2</sub>. The PXRD pattern of washed MT-ZnSiN<sub>2</sub>, shown in 1(b), was obtained from products synthesized by solid-state metathesis reaction according to the formal reaction equation:



Solid-state metathesis reactions have recently been applied for various ion-exchange reactions as a powerful tool to access metastable or kinetically hindered phases. These reaction pathways have been found to be especially useful for the synthesis of novel nitridosilicates and nitridoaluminates, which are challenging to access by conventional solid-state synthesis methods.<sup>[22,23]</sup> The PXRD pattern resulting from the reaction product can be clearly attributed to a II-IV-V<sub>2</sub> compound, corresponding to ZnSiN<sub>2</sub>, as indicated by the most prominent reflections of the calculated HP-ZnSiN<sub>2</sub> structure. Both compounds crystallize in orthorhombic space group *Pna*2<sub>1</sub> (no. 33) and can be derived from the wurtzite structure type by ordering of tetrahedrally coordinated Zn<sup>2+</sup> and Si<sup>4+</sup>. This ordering can be verified by the first two superstructure reflections (110) and (011), which do not occur for ZnSiN<sub>2</sub> synthesized from molecular precursors.<sup>[24,25]</sup> The reflections of MT-ZnSiN<sub>2</sub> are found to be fairly broad, indicating the small particle size of the resulting product pictorially highlighted by TEM. The crystallinity of MT-ZnSiN<sub>2</sub> could not be improved by the use of excess LiCl (flux method) or by longer annealing periods of the products. Instead MT-ZnSiN<sub>2</sub> was found to decompose, when reacted for longer than the optimal reaction time of one hour at 900 °C. MT-ZnSiN<sub>2</sub> was found to be white in color with a faint yellow touch. The cell parameters of MT-ZnSiN<sub>2</sub> for space group *Pna*2<sub>1</sub> were determined by a LeBail-fit<sup>[26]</sup> and are  $a \approx 5.2578(9)$  Å,  $b \approx 6.303(2)$  Å, and  $c \approx 5.0287(9)$  Å.

In Figure 1c, we show the PXRD pattern of HP-ZnSiN<sub>2</sub>, which was synthesized by annealing of the MT-ZnSiN<sub>2</sub> at a pressure of 6 GPa and a temperature of 1200 °C for 1 h. The product of this annealing reaction is found to be single phase ZnSiN<sub>2</sub> with very sharp reflections, indicating a high crystallinity. The cell parameters of the HP-ZnSiN<sub>2</sub> for space group *Pna*2<sub>1</sub> were determined by a LeBail-fit and are  $a \approx 5.24673(3)$  Å,  $b \approx 6.27941(6)$  Å, and  $c \approx 5.02249(2)$  Å. The fitted PXRD pattern of HP-ZnSiN<sub>2</sub> is shown in Figure 1d, with the most prominent reflections indexed and extended as dotted lines to the observed diffraction pattern of MT-ZnSiN<sub>2</sub> and HP-ZnSiN<sub>2</sub> matching the ones in the calculated diffraction pattern. For the sample synthesized under high pressure, all lattice parameters are slightly smaller than MT-ZnSiN<sub>2</sub>, which was synthesized at significantly lower pressure.

### TEM of ZnSiN<sub>2</sub>

For comparison of the crystal shape and the crystal size of MT-ZnSiN<sub>2</sub> and HP-ZnSiN<sub>2</sub>, we have performed transmission-electron-microscopy (TEM) measurements. Specifically, we have obtained bright-field images, and performed selected area electron diffraction (SAED) and energy dispersive X-ray spectroscopy (EDX) measurements. The bright-field images of the sample obtained by high-pressure synthesis revealed very good crystallinity. The single crystals were found to be all larger than 3 μm in size. The crystallite shown in Figure 2a is representative for the whole sample. The EDX measurements confirmed the chemical composition with an average for the atomic ratio Zn:Si of 1.3:1.6. The orthorhombic metrics of space group *Pna*2<sub>1</sub> for HP-ZnSiN<sub>2</sub> was confirmed by SAED

tilt-series, two representative patterns obtained along the [011] and the along [112] directions with some highlighted reflections are shown in Figure 2b and d.

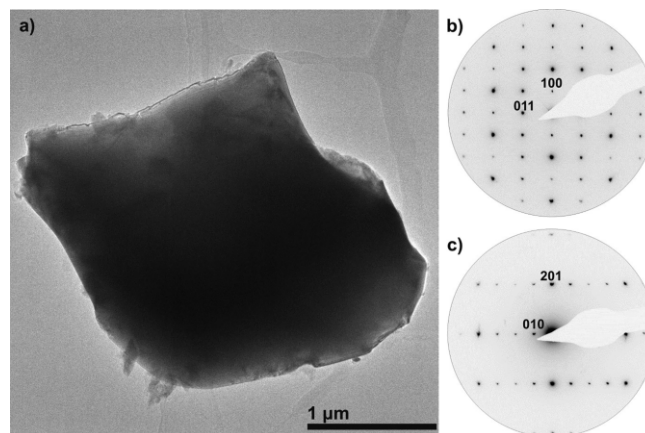


**Figure 2.** (a) Bright-field image of representative HP-ZnSiN<sub>2</sub> crystal out of the sample obtained by high-pressure synthesis. (b) Experimental SAED patterns along [011] and (c) along [112] directions with exemplary reflections labeled with indices.

Due to the broad reflections in the PXRD pattern of the sample from solid-state metathesis reaction, the crystal size of MT-ZnSiN<sub>2</sub> can be expected not to exceed the sub-micron or even the nanometer range. This assumption was verified by our TEM measurements. With bright-field images, we observed two morphologies for the MT-ZnSiN<sub>2</sub> sample. On the one hand we found geometrically ill-defined nanometer-size grains with a maximum diameter of 50 nm, on the other hand, we observed well-defined needle shaped nanometer-sized crystals with a maximum length of 500 nm. However, the diffraction volume is low in both cases, resulting in challenging diffraction data. Representative bright-field images of the nanometer sized grains are shown in Figure 3a, while the nanometer sized needle-like crystals are shown in Figure 3c. The observed

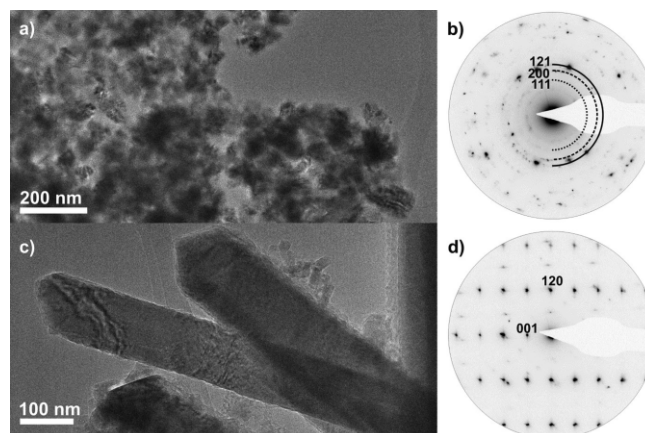


**Figure 3.** Bright-field images of representative particles of the MT-ZnSiN<sub>2</sub> sample, consisting of (a) nano-sized grains and (c) of needle-shaped nano-crystals. The corresponding experimental SAED patterns are shown for (b) the nano-sized grains and for the (d) needle-shaped nano-crystals. All SAED patterns were taken along the [210] directions, and exemplary reflections are labeled with indices.

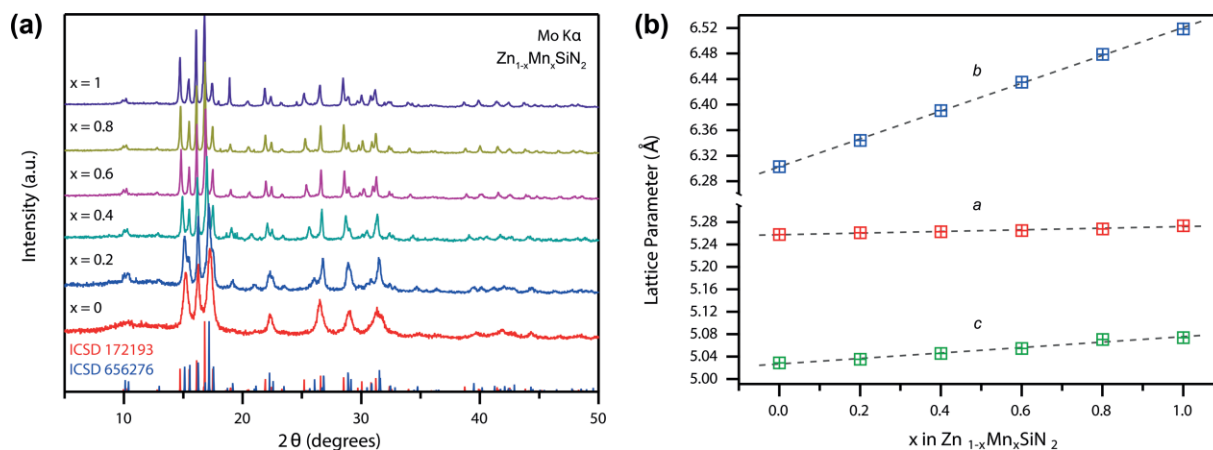
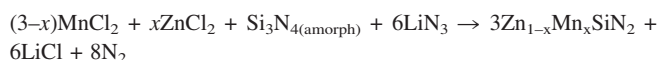


**Figure 4.** (a) PXRD pattern of the  $Zn_{1-x}Mn_xSiN_2$  solid solution for  $x = 0.0, 0.2, 0.4, 0.6, 0.8, 1.0$  synthesized by means of solid-state metathesis, with the theoretical PXRD pattern depicted on the bottom of the Figure. (b) Evolution of cell parameters of the  $Zn_{1-x}Mn_xSiN_2$  solid solution as a function of composition.

SAED are displayed in Figure 3b for the nanometer-sized grains and in Figure 3d for the needle-like nano-crystals. The observed metric of both morphologies correspond very well with the orthorhombic structure model of  $ZnSiN_2$ . For the nano-sized grains reflections (111), (200), and (121) along the [210] direction are marked in the Figure for the isotropically averaged values. In the case of the needle-shaped nano-crystals the SAED pattern can be fully indexed along the [210] direction. Within the accuracy of EDX, we find particles of both morphologies to be in agreement with a chemical composition that corresponds in average to an atomic ratio Zn:Si = 1.1:1.8.

### The $ZnSiN_2$ - $MnSiN_2$ Solid Solution

By means of solid-state metathesis reaction, we find the whole  $ZnSiN_2$ - $MnSiN_2$  solid solution to be accessible. All samples were synthesized according to the general formula:



The PXRD pattern of the synthesized products of the series  $Zn_{1-x}Mn_xSiN_2$  for  $x = 0.0, 0.2, 0.4, 0.6, 0.8, 1.0$  are depicted in Figure 4a. All samples are found to be of single phase with no additional reflections after washing and no splitting of any of the reflections. This indicates complete miscibility for the entire range of the solid solution. For the solid solution members close to  $ZnSiN_2$  composition we find broad reflection peaks, corresponding to the nano-size grains (as discussed for MT- $ZnSiN_2$ , above). For increasing manganese content the reflections become sharper, which corresponds to an increasing crystallinity of the samples. The linearly increasing cell parameters are illustrated in Figure 4b. All lattice parameters follow Vegard's law as it is expected for this type of isostructural solid solution.<sup>[27]</sup>

The bandgap evolution across the solid solution series was investigated by diffuse reflectance spectroscopy (Figure S1, Supporting Information) and is illustrated in Figure 5. The Kubelka-Munk function  $F(R) = (1-R)^2/2R$  with  $R$  = reflectance

was used to calculate pseudo-absorption spectra.<sup>[28]</sup> The subplot in Figure 5 illustrates the Tauc plots which were used for bandgap determination, assuming a direct transition for each sample.<sup>[29]</sup> The observed absorption bands in the spectra of  $ZnSiN_2$  and  $MnSiN_2$  were primarily attributed to direct transitions due to the similarity of direct and indirect bandgaps in the materials.<sup>[16,21]</sup> Direct transitions for the solid solutions were assumed according to previously reported DFT calculations.<sup>[17]</sup> The bandgap of the boundary phases  $ZnSiN_2$  (3.7 eV), and  $MnSiN_2$  (3.4 eV) are well between the range expected from literature,<sup>[16,21]</sup> and the bandgap of the solid solution  $Zn_{1-x}Mn_xSiN_2$  is linearly decreasing with increasing  $x$ . Again, following the trend expected for this kind of solid solution and stressing the tunability of the bandgap.

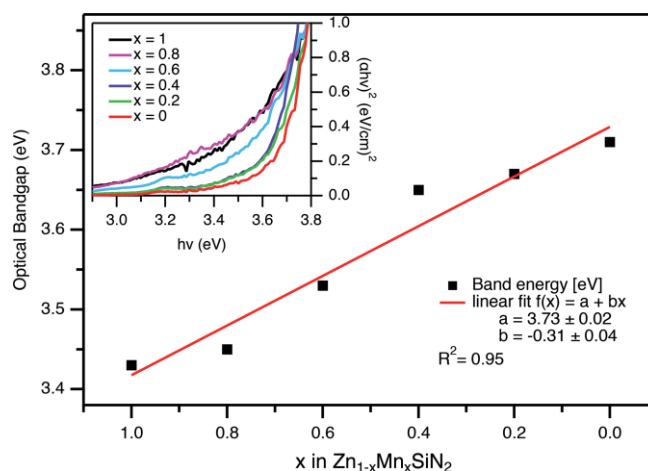


**Figure 5.** Bandgap evolution in  $Zn_{1-x}Mn_xSiN_2$  as obtained from UV/Vis measurements. The top left sup-plot illustrates the Tauc plots for each solid solution and was used for bandgap evaluation.

By incorporating a small amount (ca. 5%) of  $Mn^{2+}$  into the  $ZnSiN_2$  host lattice, we expected broad red emission, which was earlier assigned to the  ${}^4T_1 \rightarrow {}^6A_1$  transition of the  $Mn^{2+}$  ion in this type of host lattice.<sup>[30]</sup> Emission from  $Mn^{2+}$  ions has been reported for the isostructural host lattices  $ZnSiN_2$ ,

ZnGeN<sub>2</sub>, and MgSiN<sub>2</sub>.<sup>[31,32]</sup> The sample with nominal composition MT-Zn<sub>0.95</sub>Mn<sub>0.05</sub>SiN<sub>2</sub> synthesized by means of solid-state metathesis reaction does, however, not show any photoluminescence properties, for any of the tested excitation wavelengths within a range of 250 nm <  $\lambda_{\text{excitation}}$  < 600 nm. Only after annealing the MT-sample at a pressure of 6 GPa and a temperature of 1200 °C for 1 h, we found the sample to be an intense red emitter with maxima in the excitation spectra at  $\lambda_{\text{exc}} \approx 255$  nm and a broad emission maximum at  $\lambda_{\text{max,emi}} \approx 619$  nm. The photoluminescence excitation and emission spectra of ZnSiN<sub>2</sub>:Mn<sup>2+</sup> at room temperature are shown in Figure 6. The dominating excitation band can be ascribed to the host absorption transition.

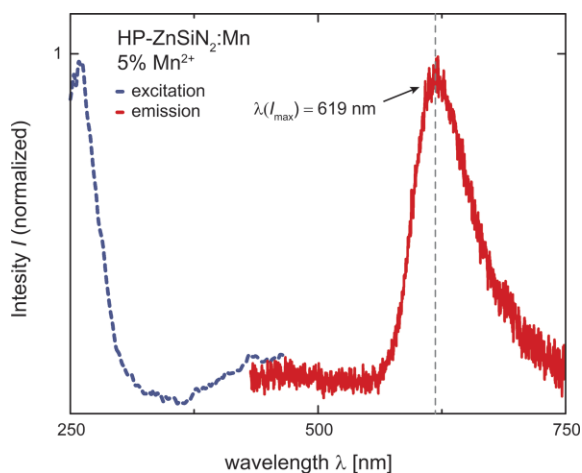


**Figure 6.** Photoluminescence excitation and emission spectra of the high-pressure annealed Zn<sub>0.95</sub>Mn<sub>0.05</sub>SiN<sub>2</sub> sample.

## Conclusions

We have reported on the synthesis of the II-IV-N<sub>2</sub> semiconductors ZnSiN<sub>2</sub>, MnSiN<sub>2</sub>, and the Zn<sub>1-x</sub>Mn<sub>x</sub>SiN<sub>2</sub> solid solution by a one-step solid-state metathesis reaction. We have shown that these compounds can be obtained by reacting the corresponding metal halides with stoichiometric amounts of silicon nitride and lithium azide. All obtained phases could be indexed using the orthorhombic space group *Pna*2<sub>1</sub>, corresponding to the wurtzite-type superstructure.

We have found that this reaction pathway yields single phase products without applying external pressure and at a moderate reaction temperature of 700 °C and states a more accessible reaction pathway for ZnSiN<sub>2</sub>. The resulting ZnSiN<sub>2</sub> was found to consist of nano-sized grains and needle-shaped nano-crystals, resulting in a PXRD pattern with broad reflections. With increasing manganese content in the Zn<sub>1-x</sub>Mn<sub>x</sub>SiN<sub>2</sub> solid solution, we found the reaction product to be increasingly crystalline. Both the cell parameters and the bandgap across the different compositions of the solid solution change linearly, displaying good optical bandgap tunability, and resulting in a possible changeability of properties. The sample Zn<sub>0.95</sub>Mn<sub>0.05</sub>SiN<sub>2</sub> synthesized by means of solid-state metathesis reaction becomes an intense red emitter with a broad emission maximum

at  $\lambda_{\text{emission}} = 619$  nm when excited with ultraviolet light after annealing the sample at a pressure of 6 GPa and a temperature of 1200 °C. The complete solid solution represents a continuous transition from a Mn<sup>2+</sup> [Ar]3d<sup>5</sup> configuration to a Zn<sup>2+</sup> [Ar]3d<sup>10</sup> configuration, which potentially could be the subject of a more detailed study of the strong magnetic interactions due to superexchange.

## Acknowledgements

The project was funded by the Deutsche Forschungsgemeinschaft (DFG, German Research Foundation) under Germany's Excellence Strategy – EXC 2089/1–390776260. FvR acknowledges financial support from the Swiss National Science Foundation under Grant No. PZ00P2174015. The authors gratefully acknowledge *Mathias Mallmann* (Department of Chemistry, LMU) for inspiring discussions.

**Keywords:** Solid solution series; Solid-state metathesis; Nitrides; Semiconductors

## References

- [1] K. Shinohara, D. C. Regan, Y. Tang, A. L. Corrion, D. F. Brown, J. C. Wong, J. F. Robinson, H. H. Fung, A. Schmitz, T. C. Oh, S. J. Kim, P. S. Chen, R. G. Nagele, A. D. Margomenos, M. Micovic, *IEEE Trans. Electron Devices* **2013**, *60*, 2982–2996.
- [2] S. P. DenBaars, D. Feezell, K. Kelchner, S. Pimpitkar, C.-C. Pan, C.-C. Yen, S. Tanaka, Y. Zhao, N. Pfaff, R. Farrell, M. Iza, S. Keller, U. Mishra, J. S. Speck, S. Nakamura, *Acta Mater.* **2013**, *61*, 945–951.
- [3] F. Dimroth, *Phys. Status Solidi C* **2006**, *3*, 373–379.
- [4] V. L. Shaposhnikov, A. V. Krivosheeva, V. E. Borisenko, *Phys. Rev. B* **2012**, *85*, 205201.
- [5] A. J. Spring-Thorpe, B. R. Pamplin, *J. Cryst. Growth* **1968**, *3*, 313–316.
- [6] W. Frederick, C. L. Tang, *Phys. Rev. B* **1973**, *8*, 4607–4611.
- [7] J. Wu, W. Walukiewicz, *Superlattice Microst.* **2003**, *34*, 63–75.
- [8] A. D. Martinez, A. N. Fioretti, E. S. Toberer, A. C. Tamboli, *J. Mater. Chem. A* **2017**, *5*, 11418–11435.
- [9] Y. Hinuma, T. Hatakeyama, Y. Kumagai, L. A. Burton, H. Sato, Y. Muraba, S. Iimura, H. Hiramatsu, I. Tanaka, H. Hosono, F. Oba, *Nat. Commun.* **2016**, *7*, 11962.
- [10] S. Esmailzadeh, U. Halenius, M. Valldor, *Chem. Mater.* **2006**, *18*, 2713–2718.
- [11] P. C. Quayle, K. He, J. Shan, K. Kash, *MRS Commun.* **2013**, *3*, 135–138.
- [12] A. Punya, W. R. L. Lambrecht, M. van Schilfhaarde, *Phys. Rev. B* **2011**, *84*, 165204.
- [13] F. Kawamura, N. Yamada, M. Imai, T. Taniguchi, *Cryst. Res. Technol.* **2016**, *51*, 220–224.
- [14] T. Endo, Y. Sato, H. Takizawa, M. Shimada, *J. Mater. Sci. Lett.* **1992**, *11*, 424–426.
- [15] A. Mintairov, J. Merz, A. Osinsky, V. Fuflyigin, L. D. Zhu, *Appl. Phys. Lett.* **2000**, *76*, 2517–2519.
- [16] J. Häusler, S. Schimmel, P. Wellmann, W. Schnick, *Chem. Eur. J.* **2017**, *23*, 12275–12282.
- [17] M. Mallmann, R. Niklaus, T. Rackl, M. Benz, T. G. Chau, D. Johrendt, J. Minár, W. Schnick, *Chem. Eur. J.* **2019**, *25*.
- [18] N. Hofman-Bang, *Acta Chem. Scand.* **1957**, *11*, 581–582.
- [19] H. Huppertz, *Z. Kristallogr., Cryst. Mater.* **2004**, *219*, 330–338.
- [20] B. Toby, R. B. V. Dreele, *J. Appl. Crystallogr.* **2013**, *46*, 544–549.
- [21] J. Häusler, R. Niklaus, J. Minár, W. Schnick, *Chem. Eur. J.* **2018**, *24*, 1686–1693.

- [22] P. Strobel, S. Schmiechen, M. Siegert, A. Tücks, P. J. Schmidt, W. Schnick, *Chem. Mater.* **2015**, *27*, 6109–6115.
- [23] P. Bielec, O. Janka, T. Block, R. Pöttgen, W. Schnick, *Angew. Chem.* **2018**, *130*, 2433–2436; *Angew. Chem. Int. Ed.* **2018**, *57*, 2409–2412.
- [24] E. W. Blanton, K. He, J. Shan, K. Kash, *J. Cryst. Growth* **2017**, *461*, 38–45.
- [25] J. Engering, M. Jansen, *Z. Anorg. Allg. Chem.* **2003**, *629*, 109–115.
- [26] A. Le Bail, H. Duroy, J. L. Fourquet, *Mater. Res. Bull.* **1988**, *23*, 447–452.
- [27] A. R. Denton, N. W. Ashcroft, *Phys. Rev. A* **1991**, *43*, 3161–3164.
- [28] R. López, R. Gómez, *J. Sol-Gel Sci. Technol.* **2012**, *61*, 1–7.
- [29] J. Tauc, R. Grigorovici, A. Vancu, *Phys. Status Solidi* **1966**, *15*, 627–637.
- [30] K. Uheda, H. Takizawa, T. Endo, C. Miura, Y. Shimomura, N. Kijima, M. Shimada, *J. Mater. Sci. Lett.* **2001**, *20*, 1753–1755.
- [31] C. J. Duan, A. C. A. Delsing, H. T. Hintzen, *J. Lumin.* **2009**, *129*, 645–649.
- [32] Q.-H. Zhang, J. Wang, C.-W. Yeh, W.-C. Ke, R.-S. Liu, J.-K. Tang, M.-B. Xie, H.-B. Liang, Q. Su, *Acta Mater.* **2010**, *58*, 6728–6735.

---

Received: November 30, 2019

Published Online: February 3, 2020